J Mol Model (2012) 18:4665–4673
DOI 10.1007/s00894-012-1464-6

ORIGINAL PAPER

Binding mechanism between Hsp90 and Sgt1 explored by homology modeling and molecular dynamics simulations in rice

Jun-jie Yan · Yu-bo Zhang · Yi Ding

Received: 18 October 2011 / Accepted: 11 May 2012 / Published online: 1 June 2012

Abstract The Hsp90 (for heat shock protein90) and the Sgt1 (for suppressor of the G2 allele of *skp1*) are widely distributed in animals, yeast, and plants. The former functions as molecular chaperon activating a series of client proteins, the latter functions as an adaptor protein participating in multiple biological processes such as immunity response through interactions with different protein complexes. In the present study, we have constructed a homology model of Hsp90-Sgt1 complex in rice based on a recently resolved structure from barley and *Arabidopsis* to explore its binding mechanisms and to understand the detailed interaction profile. A total of 20 ns explicit solvent molecular dynamics simulations combined with MM-GBSA computations and virtual alanine scanning were performed for the modeled complex. In the final structure, three strong salt bridges were found between OsHsp90 and OsSgt1, D217(OsHsp90) - K186(OsSgt1), D218(OsHsp90) - K237 (OsSgt1) and K161(OsHsp90) - E239(OsSgt1). Besides, residue Y173 of OsSgt1 played a vital role in the interactions with OsHsp90, the detailed interactions were discussed. These results would help us understand the critical features determining the Hsp90-Sgt1 binding process.

Keywords Homology modeling · Hsp90 · MD simulations · MM-GBSA · Sgt1

Electronic supplementary material The online version of this article (doi:10.1007/s00894-012-1464-6) contains supplementary material, which is available to authorized users.

J.-j. Yan · Y.-b. Zhang · Y. Ding (✉)
State Key Laboratory of Hybrid Rice, Department of Genetics, College of Life Sciences, Wuhan University, Wuhan 430072, People's Republic of China
e-mail: yiding@whu.edu.cn

Abbreviations

RMSD	Root mean square deviation
MD	Molecular dynamics
Rg	Gyration radius
Hsp90	Heat shock protein90
Sgt1	Suppressor of the G2 allele of skp1

Introduction

The Hsp90 (for heat shock protein90) is a kind of quite conserved protein found from prokaryotic cells to eukaryotic cells including humans and plants, which is composed of three regions: an N-terminal nucleotide binding domain containing an ATP binding module, a middle client binding domain, and a C-terminal dimerization domain [1, 2]. As molecular chaperon, it not only involves identifying misfolded proteins under stress situations, but also functions under normal conditions in many cellular processes including protein folding, protein degradation, stability of the client proteins which are key components for cellular signal transduction [3, 4]. In human, as many of the Hsp90 client proteins participate in the tumor cell growth, to find some new inhibitors on Hsp90 to control cancer cell proliferation is expected to be an ideal way for cancer therapy [5–8]. Besides, Hsp90 is also found to form complexes with various proteins such as transcription factors, steroid hormone receptors, tyrosine and serine kinases to regulate basic cell process [9–11].

Sgt1(for suppressor of G2 allele of *skp1*) is also a kind of conserved protein which is widely distributed in animals, yeast and plants, and it is composed of three conserved domains: an N-terminal TPR (tetratricopeptide repeat) domain, a central CS (CHORD-Sgt1) domain, and a C-terminal SGS (Sgt1-specific) domain [12]. In human, two

isoforms of Sgt1, Sgt1a and Sgt1b, are both important for the kinetochore assembly as in the yeast [13]. Knockdown of Sgt1 protein would cause immunodeficiency for humans to be infected by bacterial PGN [14]. As for plants, *Arabidopsis* also contains two Sgt1 isoforms, Sgt1a and Sgt1b, which double mutant would lead to embryo lethal in *Arabidopsis*, suggesting that Sgt1 proteins are essential for the plant development [15]. Besides, Sgt1 were also found involved in the immunity responses in *Arabidopsis* [16].

Interactions between Sgt1 and Hsp90 are found in a wide range species and the interactions are required for R protein accumulation and invoking immunity responses [17]. Both NMR structural and mutagenesis analysis indicate that only the CS domain of Sgt1 is sufficient to bind with the N terminal of Hsp90 in human and in plants [18, 19]. Moreover, the crystal structure of N-Hsp90-Sgt1-CS complex is determined and mutational analysis indicates that the complex exhibits a vital role in the assembly of SCF ubiquitin ligase complex [20].

Exploring the Hsp90-Sgt1 interaction details would give us new insights of how they act as immunity sensors. Further more, it might be useful for drug design targeting Hsp90 against tumor cells in humans. However, the dynamic interactions between Hsp90 and Sgt1 is not clear in plants. In recent years, molecular dynamics (MD) simulations have been widely used to study protein-protein interactions, which would provide not only the dynamic properties of complex in solution among large time scales, but also a wealth of energetic information between protein interactions [21–23]. In the present study, we aimed to explore the interaction features about the Hsp90-Sgt1 complex in rice. The complex of Hsp90 N-terminus and Sgt1 CS domain in rice was obtained by homology modeling. Reliability of the complex was validated by 20 ns explicit solvent MD simulations in combination with MM-GBSA and virtual alanine scanning computational method. Detailed interaction profile of the complex was further explored by pairwise distance and energy analysis for critical residues based on the molecular dynamics trajectory. The final equilibrium structure and trajectory analysis showed that the salt bridges and hydrogen bonds played important roles in the stability of the complex in rice.

Materials and methods

Preparation of the starting structure

Rice Hsp90 (GI: 6863054) and Sgt1 (GI: 6581058) sequences were downloaded from NCBI website. Coordinates of Barley Hsp90 N-terminal and *Arabidopsis* Sgt1 CS domain were obtained from protein data bank (PDB code: 2JKI) [20]. Complex of Hsp90-N (75aa-290aa) and Sgt1-CS (167aa-256aa) from rice (OsHsp90 and OsSgt1) was modeled using SWISS-MODEL based on the structure of 2JKI as they showed considerably high sequence similarities through alignment (Supplemental Fig. 1a and 1b). The alignment was executed by ClustalW [24].

Computational alanine scanning

Molecular mechanics Poisson-Boltzmann surface area (MM-PBSA) method [25] had become a commonly used approach to estimate binding free energy of protein partners. MM-GBSA [26], a variant of MM-PBSA, which replaced PB electrostatics with the generalized Born (GB) approximate model of electrostatics was faster and had aroused great interest in binding free energy calculations [21, 27–30]. To verify the quality and validity of the modeled complex, 100 ps GB (IGB=2) molecular dynamics simulations instead of explicit water was performed using AMBER11 [31] software packages along the 50,000 steps. Before the 100 ps unrestrained production run, energy minimization was conducted using 500 steps steepest descent method followed by another 500 steps conjugate gradient to remove spacial clashes. Besides, 100 ps GB MD simulations were also carried out for the 20 ns refined structure and the crystal structure of 2JKI in the same way as the modeled structure. The ff99 forcefield (Parm99) [32] was applied throughout energy minimization and molecular dynamics simulations. The time step of molecular dynamics simulations was 2 fs with a nonbond cutoff of 10 Å. Langevin dynamics with a collision frequency of 2.0 ps^{-1} was employed to control the temperature of the system. The SHAKE algorithm was applied to constrain all bonds involving hydrogen [33]. The relative binding free energy $\Delta G^{*}_{binding}$ was calculated by using MM-PBSA module of amber11 [31]. The binding free energy of A + B → AB was calculated using the following thermodynamic cycle: (Scheme1)

Where T is the temperature, S is the solute entropy, ΔG_{gas} is the interaction energy between A and B in the gas phase, and ΔG^{A}_{solv}, ΔG^{B}_{solv}, and ΔG^{AB}_{solv} are the solvation free energies of A, B, and AB, which are estimated using a GB surface area (GBSA) method [34, 35]. That is, $\Delta G^{AB}_{solv} = \Delta G^{AB}_{GBSA} + \Delta G^{AB}_{GB} + \Delta G^{AB}_{SA}$, and so forth. ΔG_{GB} and ΔG_{SA} are the electrostatic and nonpolar terms, respectively. The bond, angle, and torsion energies constitute the intramolecular energy ΔE_{intra} of the complex, while ΔE_{elec} and ΔE_{vdw} represent the receptor-ligand electrostatic and Van der Waals interactions, respectively. Because of the constant contribution of $-T\Delta S$ for each complex, we refer to $\Delta G^{*}_{binding}$ for $\Delta G_{binding} + T\Delta S$ in the discussion. The post processing ten snapshots from the trajectory were generated to calculate the

Scheme 1 Thermodynamic cycle scheme for binding free energy calculations between OsHsp90 and OsSgt1

$$\begin{array}{ccccc} A_{aqu} & + & B_{aqu} & \xrightarrow{\Delta G_{binding}} & AB_{aqu} \\ \Big\downarrow -\Delta G^{A}_{solv} & & \Big\downarrow -\Delta G^{B}_{solv} & & \Big\downarrow -\Delta G^{AB}_{solv} \\ A_{gas} & + & B_{gas} & \xrightarrow{\Delta G_{gas}} & AB_{gas} \end{array}$$

$$\begin{aligned} \Delta G_{binding} &= \Delta G_{gas} - \Delta G^{A}_{solv} - \Delta G^{B}_{solv} + \Delta G^{AB}_{solv} \\ &= \Delta H_{gas} - T\Delta S - \Delta G^{A}_{GBSA} - \Delta G^{B}_{GBSA} + \Delta G^{AB}_{GBSA} \\ &= \Delta H_{gas} - T\Delta S + \Delta\Delta G_{GB} + \Delta\Delta G_{SA} \end{aligned}$$

$$\Delta H_{gas} \approx \Delta E_{gas} = \Delta E_{intra} + \Delta E_{elec} + \Delta E_{vdw}$$

$$\Delta\Delta G_{GB} = \Delta G^{AB}_{GB} - \left(\Delta G^{A}_{GB} + \Delta G^{B}_{GB}\right)$$

$$\Delta\Delta G_{SA} = \Delta G^{AB}_{SA} - \left(\Delta G^{A}_{SA} + \Delta G^{B}_{SA}\right)$$

binding free energy of the system. Important residues participating in the interactions validated in the Y2H assay [20] were mutated into alanine, and the relative binding free energy $\left(\Delta\Delta G^{*}_{binding}\right)$ was calculated between the wildtype and the mutated.

Molecular dynamics simulations

GROMACS4.5.3 [36] software package with OPLS/AA forcefield [37] was used to perform a total of 20 ns explicit solvent molecular dynamics simulations for the modeled complex to introduce the solvent effect. The simulation steps were carried out as follows.

Firstly, the system was solvated in the single point charge (SPC216) water in a cubic box with a 1.0 nm solute-wall minimum distance. Counterions were added to compensate the net charge of the system to a final concentration of 0.1 M. Secondly, 1000 steps energy minimization was performed to remove spacial clashes of the complex using steepest descent method. Then 100 ps molecular dynamics simulations with position restraints with a force constant of 1000 kJ mol^{-1} nm^{-2} on the complex were applied, which enables the water to pack around the protein. Lastly, three independent 20 ns molecular dynamics simulations (Q1, Q2, Q3) were carried out with the same conditions except that all position restraints were removed.

The system was coupled to an external bath by the Berendsen [38] temperature and pressure method with a time constant of τ_T=0.1 ps and τ_P=1 ps respectively. Long-range electrostatic interactions beyond the cutoff were treated with the Partical-mesh Ewald (PME) algorithm [39] and van der Waals was applied with a cut-off distance of 1.0 nm. The linear constraint (LINCS) [40] algorithm was used to constrain all bond lengths to their equilibrium positions. All MD simulations were with a time step of 2 fs. The final trajectory was analyzed by the standard tools provided by GROMACS software package. Structure visualization and manipulation was performed using VMD1.8.7 [41] and PyMOL (http://www.pymol.org/). The pairwise distance and energy analysis was accomplished using R language (http://www.r-project.org/).

Results and discussion

Homology modeling of rice Hsp90 and Sgt1 complex and its structure characteristics

Sequence alignment between OsHsp90-N(75-290aa)-OsSgt1-CS(4-217aa) and 2JKI showed 60 % sequence similarity (Supplementary Fig. 1a, 1b). Thus we modeled the OsHsp90-N-OsSgt1-CS complex in rice based on the structure of 2JKI using Swiss-model online service, and the complex was obtained as shown in Fig. 1b. For the modeled structure (Fig. 1b), OsSgt1 bound with OsHsp90 using its four anti-parallel β sheets as displayed in the structure of 2JKI (Fig. 1a). Comparing the modeled structure with the

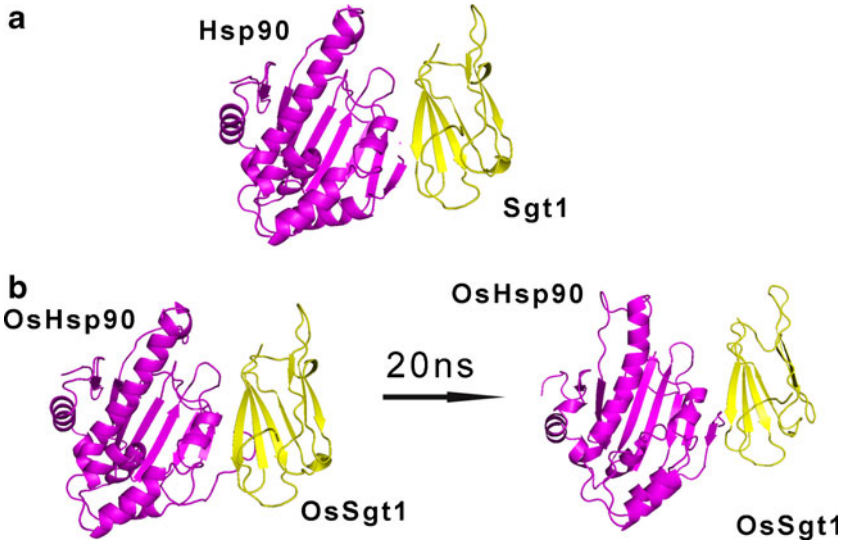

Fig. 1 Structure information of the Hsp90-Sgt1 complex. Crystal structure of 2JKI (**a**); The modeled OsHsp90-OsSgt1 complex from rice based on the structure of 2JKI and the final refined structure after 20 ns molecular dynamics simulations (**b**)

structure of 2JKI, the most obvious difference was that the first eight residues in OsHsp90 were shown as a coil in the modeled structure but it displayed as a β-sheet in 2JKI.

Stability analysis during explicit solvent molecular dynamics simulations

To validate the stability of the structure and to introduce the solvent effect, we performed 20 ns explicit solvent molecular dynamics simulations for the modeled complex. Here, the equilibration of the MD trajectories was monitored from the convergence of the Cα root mean square deviation (RMSD) with respect to the equilibrium structure just prior to the production molecular dynamics simulations (Fig. 2a). From Fig. 2a, it could be seen that the relative fluctuation was small and the system had reached equilibrium around 2.7 Å after 6 ns simulations. Potential energy was important for the complex stability. The lower the energy and fluctuation, the more stability for the complex. Thus the potential energy of our modeled complex along the trajectory was checked. It showed a rather favorable low value with an average of -696000 kJ mol^{-1} (Fig. 2b). The gyration radius (Rg) of the complex was calculated because the gyration radius of a protein was a measure of its compactness, which maintained a relatively steady value around 2.15 nm along the simulations (Fig. 2c). The Cα RMSD and Rg for Q2 and Q3 simulations were shown in Supplementary materials (Supplementary Fig. 2). In addition, we also had gauged solvent accessible surface area of the complex, OsHsp90, OsSgt1 and the difference between them, which all showed

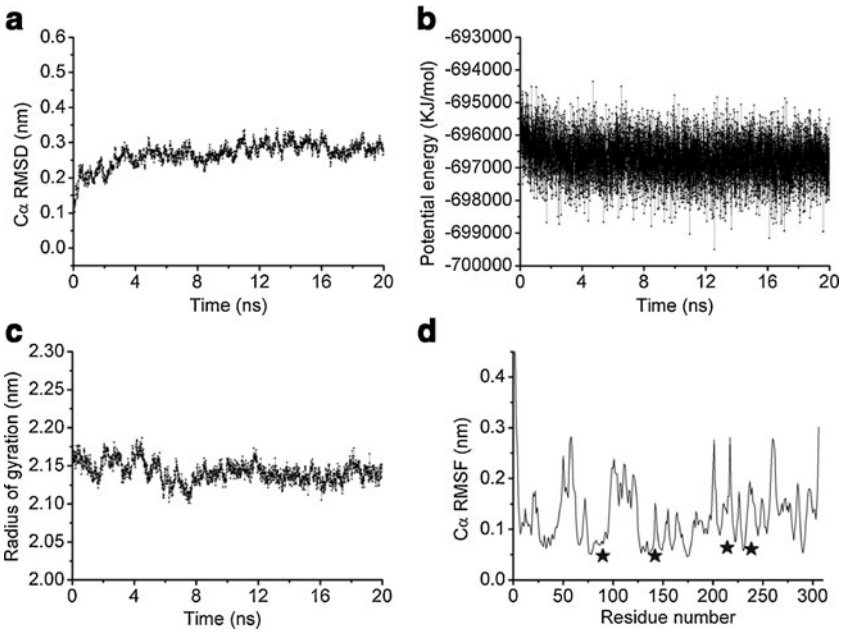

Fig. 2 Structure stability during 20 ns Q1 molecular dynamics simulations. The Cα RMSD (**a**), potential energy (**b**), gyration radius (**c**) of the system as a function of time. Root mean square fluctuations related to the average positions of the Cα atoms as a function of residue numbers. Critical residues numbers are labeled with star symbols (**d**)

a steady value (Supplementary Fig. 3). The above results confirmed that our simulation had obtained convergence along the 20 ns production run.

Secondary structure analysis

To further monitor the stability of OsHsp90-OsSgt1 complex and obtain more detailed information of the structure transformation during the simulations, the variation in secondary structure was calculated (Fig. 3), which showed that most of the secondary structure remained quite stable with only little fluctuations except for the first eight residues. As illustrated above, in our modeled structure (Fig. 1b), the first eight residues were shown as a coil, but they immediately transformed to β sheets since the simulations began and became rather stable after 2 ns simulations (Fig. 3). Such change was also validated by the results of per-residue root mean square fluctuation (RMSF) (Fig. 2d), as the first ten residues showed a considerably high value of RMSF. While little fluctuation was monitored for residues E80, K161, E162, I165, and D218 of OsHsp90 as well as residues Y173, F184, K237 and E239 of OsSgt1 displayed with a star symbol in Fig. 2d. In the previous study [20], the above residues were all on the interface of both proteins and involved in the interactions either in hydrophobic or polar interactions between the protein partners, thus our RMSF results agreed well with the previous experimental results. Therefore, it validated that our structure was equilibrated enough and quite stable along the trajectory.

Structure validated by computational alanine scanning

Site-directed mutagenesis had been widely used to identify the critical residues which were responsible for binding between the receptor and ligand [21, 27, 28, 30]. In this study, we performed virtual alanine scanning for either OsHsp90 or OsSgt1 residues for the crystal structure (2JKI), the modeled complex and the 20 ns refined structure. Three sets of computational alanine scanning results from the three individual 20 ns molecular dynamics simulations were obtained and averaged.

In the crystal structure of the 2JKI, the residues Tyr157 and Phe168 on strand one and strand two of Sgt1 formed two core hydrophobic interactions with Hsp90 [20]. In our modeled structure, Tyr173 and Phe184 correspond to the above two residues. As for Tyr173, binding free energy $\Delta\Delta G^{*}_{binding}$ showed a large value increase of 9.8 kcal mol^{-1}. However, a slower value was observed for the Phe184 with a value of 1.31 kcal mol^{-1} when mutated into alanine. Interestingly, similar results were also obtained for the crystal structures (Fig. 4). Subsequent analysis showed that Tyr173 participated in polar interactions with OsHsp90. Reports showed that the Lys221 and Glu223 mutation disrupt the interactions of Hsp90 and Sgt1 in the Y2H assay [20]. In our computational method, the binding free energy showed a great increase of 15.12 kcal mol^{-1} and 8.1 kcal mol^{-1} when the homologous residues Lys237 and Glu239 mutated to alanine respectively, which correspond well with the Y2H assay. In our model, the Tyr214 and Thr236 (corresponding residue Y199 and T220 respectively in 2JKI) resided beyond the binding interface of OsSgt1 and they had no effect on the Y2H assay, which corresponded to our computational mutation results with a considerably low value of 0 kcal mol^{-1} and 0.1 kcal mol^{-1} when mutated into alanine respectively. These results were all in agreement with the Y2H experiments.

Extensive network of polar interactions between E80, K161, D218 from OsHsp90 and K186, K237, E239 from OsSgt1 were formed around the hydrophobic interactions, which were validated by the alanine scanning results. Binding free energy all showed an increase when these residues mutated into alanine (Fig. 4). Some other residues from both OsHsp90 and OsSgt1 were mutated, most of them were consistent with each other. It was interesting to note that mutation results on D217 from OsHsp90 and R169 from OsSgt1 in the 20 ns refined structure was much closer to the crystal structure mutation, which indicated that our model had improved after 20 ns simulations. To our great interest, the mutation on E80, K161, E162 from OsHsp90 and Y173, K237, E239 from OsSgt1 in our modeled structure led to a greater increase in the binding free energy compared with the crystal structure of 2JKI, which implied that these residues might play key roles in the binding affinity in rice. Overall, very good agreements were found among the modeled structure, the 20 ns refined structure and the crystal structure.

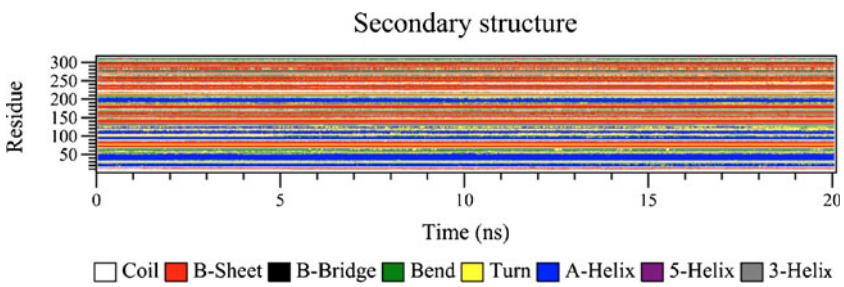

Fig. 3 Secondary structure variation during 20 ns Q1 molecular dynamics simulations for the modeled OsHsp90-OsSgt1 complex

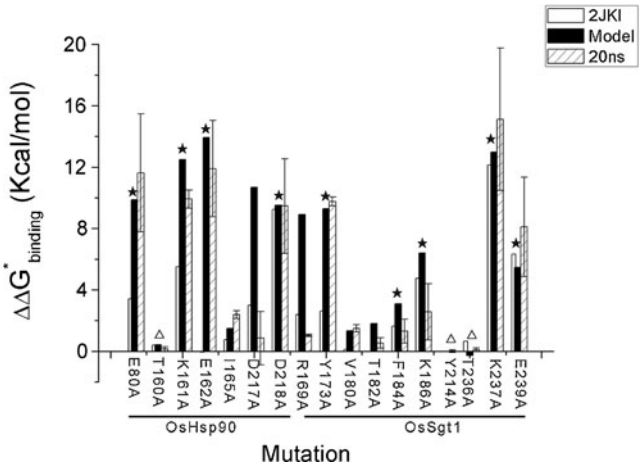

Fig. 4 Computational alanine scanning on either Hsp90 or Sgt1 residues for the crystal structure of 2JKI, the modeled structure and the 20 ns refined structure which was averaged over Q1, Q2, Q3 simulations with the standard deviation shown as error bars. Star symbol indicates residues which are important in the interactions between Hsp90 and Sgt1, while triangle symbol represents no or minor functions for the interactions as validated in the Y2H assays. Residue number is based on the OsHsp90 and OsSgt1 sequence numbers respectively

Polar interactions were critical in the complex recognition

The above alanine scanning results indicated that residues of E80, K161, D217, D218 from OsHsp90, and Tyr173, Lys186, Lys237, Glu239 from OsSgt1 might play crucial roles during the interactions of the protein partners. Among these residues, we found that there were three basic amino acids from OsHsp90 and four acidic amino acids from OsSgt1. These basic amino acids and acidic amino acids constitute the key salt bridge interactions during the simulations as shown in Fig. 5a.

Alanine scanning results for Lys186, Lys237 and Glu239 of OsSgt1 all showed a drastic increase for the binding free energy (Fig. 4), which indicated these residues might play key roles in the interactions. Thus relevant adjacent residues analysis showed that three salt bridges among D217-K186, D218-K237, K161-E239 were formed in the modeled structure (Fig. 5a). As was expected, mutation on K161, D218 from OsHsp90 showed a large increase for the binding free energy, while D217 mutation displayed a much lower value (Fig. 4). As for D217-K186, the distance varied greatly which implied that this interaction might be weaker, but the average distance was below 0.2 nm for D218-K237, K161-E239 after 7 ns simulations (Fig. 5c). Subsequently, we monitored the SR-Coulomb energy variation for these salt bridges during the simulations. As for K161-E239 and D218-K237, SR-Coulomb energy was maintained with an average value of -101.507 kJ mol^{-1} and -122.052 kJ mol^{-1} respectively. A slightly lower SR-coulomb energy was found for D217-K186, with an average value of -71.1787 kJ mol^{-1} (Fig. 5d). The above large binding free energy in combination with the alanine scanning results further demonstrated that these salt bridges played crucial roles in the complex stability.

As one of the most important forces that maintains the binding between ligand and receptor, hydrogen bonding can also reflect complex stability. We analyzed the changes in the hydrogen bonding in the binding domain of the complex. In the crystal structure of 2JKI, it had reported Y157 from Sgt1 formed hydrogen bonds with E6 and K88 of Hsp90 [20]. In our modeled structure in rice, corresponding hydrogen bond Y173(OsSgt1) - E80 (OsHsp90), Y173 (OsSgt1) - K161 (OsHsp90) was also found (Fig. 5c). The minimum distance for Y173 - K161 was rather stable along the trajectory with an average value of 0.178 nm (Fig. 5b), a stepwise SR coulomb energy calculation showed that it maintained an average value of -34.397 kJ mol^{-1}. While E80 of OsHsp90 undergoes a considerably large fluctuation for the first 2 ns (Fig. 3), the distance of Y173 - E80 reflected such variation. At the start of the run, the distance showed a larger value and fluctuated greatly until 2 ns simulations, but then remained stable at around 0.184 nm for the last 12 ns simulations (Fig. 5b). SR coulomb energy results also reflected such distance change and the value kept around -50.2494 kJ mol^{-1} for the last 12 ns (Fig. 5d).

In the previous study, Y157 and F168 from Sgt1 were reported to be important in the protein interactions and formed a hydrophobic core with Hsp90 [20]. In our study, hydrophobic interactions were also monitored for the corresponding residue of Y173 and F184. Interestingly, virtual alanine scanning results for both the crystal structure of 2JKI and the modeled structure showed that the effect of the F184 might be minor (Fig. 4). A stepwise distance and energy analysis for F184 and the surrounding residues further validated such hypothesis (Fig. 6b, c). As for Y173, distance and SR-LJ energy analysis of the two pairs Y173 - E162 and Y173 - I165 showed that they maintained an average distance value of 0.2 nm and with a binding free energy of -10 kJ mol^{-1} respectively (Fig. 6b and c) which indicated that the forces between them was rather stable.

Generality of the binding mechanism among other organisms

To further validate the generality of the interacting modes, the sequences of OsHsp90 N terminus and OsSgt1 CS domain with seven other plant species (*Zea mays*, *Hordeum vulgare*, *Glycine max*, *Nicotiana benthamiana*, *Triticum aestivum*, *Solanum tuberosum)* were aligned in our study (Supplementary Fig. 4). From Supplementary Fig. 4a, we could see that the residues K161, I165, D217, D218 of Hsp90 were all conserved. The key residues Y173, K186, K237, E239 of Sgt1 were also conserved among

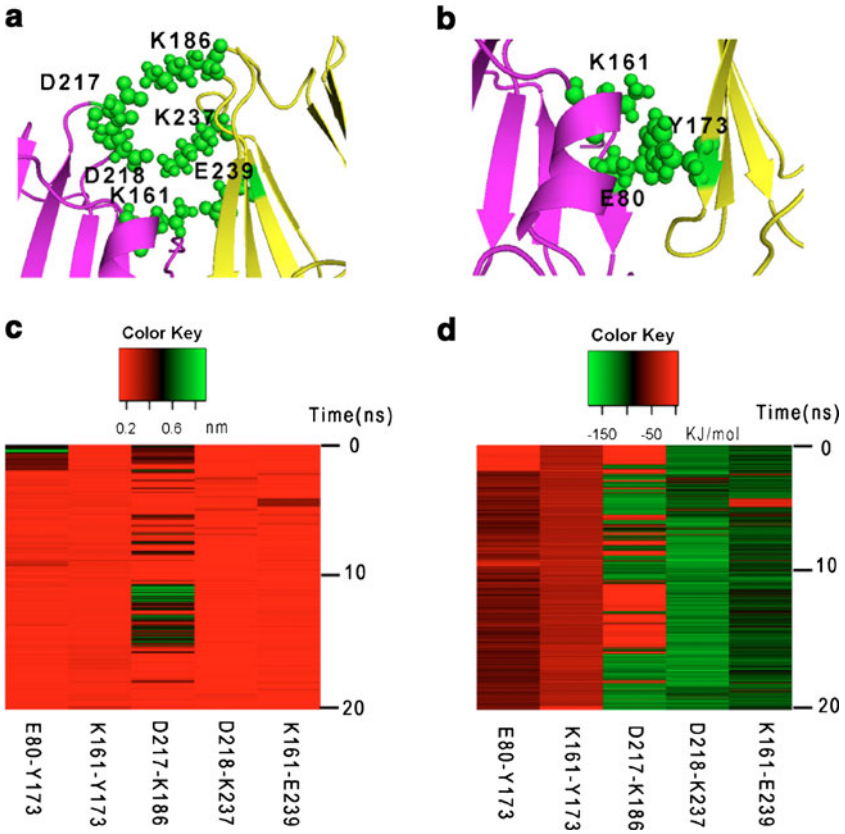

Fig. 5 Profiles of polar interactions at the interface of the protein partners for the Q1 molecular dynamics simulations. Residues involved in the salt bridge interactions (**a**) and hydrogen bond interactions (**b**) were labeled and shown in sphere in the final structure. Distance (**c**) and SR-Coulomb energy (**d**) between pairwise residues were calculated as a function of time for the 20 ns runs

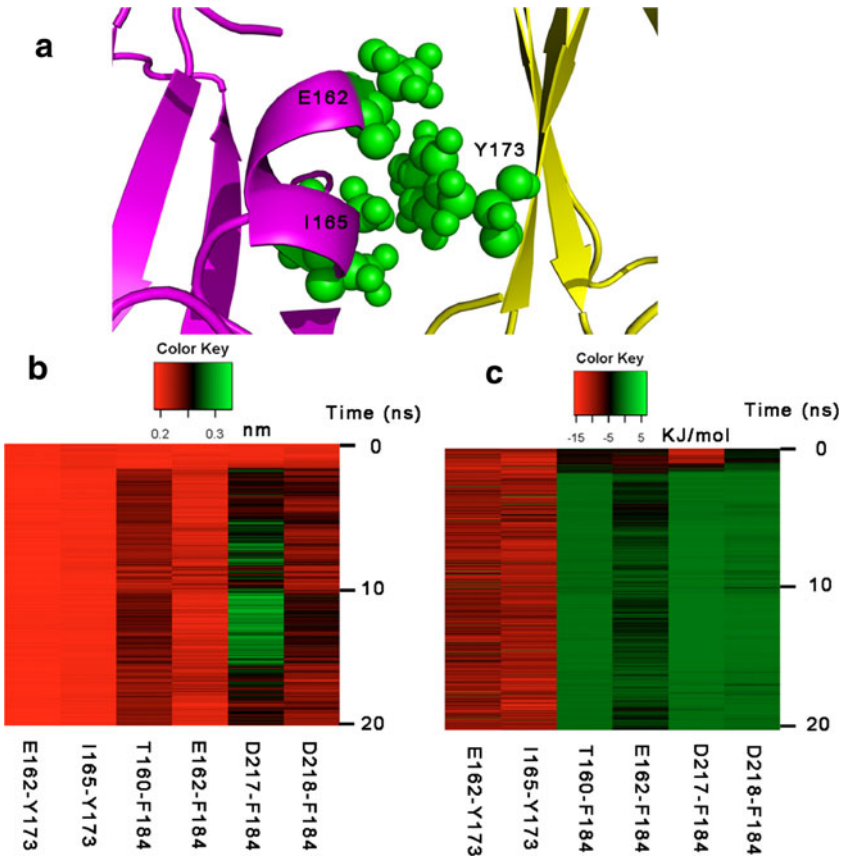

Fig. 6 Hydrophobic interaction between OsHsp90 and OsSgt1 for the Q1 molecular dynamics simulations. Key residues involved in hydrophobic interactions were labeled and shown in sphere (**a**). Distance (**b**) and SR-LJ energy (**c**) between pairwise residues were calculated as a function of time

different species. These results further illustrated that Hsp90 and Sgt1 might adopt the same binding modes among different plants.

Conclusions

In the present study, we used homology modeling method to obtain OsHsp90-OsSgt1 complex in rice. Then the structure was further refined by explicit solvent molecular dynamics simulations for a total of 20 ns. Stepwise computational alanine scanning was applied for the crystal structure of 2JKI, the modeled complex structure and the 20 ns equilibrated structure. Results showed that Tyr173 of OsSgt1 played key roles in the interactions, as it was not only participating in the hydrophobic interactions but also involved in a hydrogen bonding network with OsHsp90. Besides, three robust salt bridges were observed through the trajectory between OsHsp90 and OsSgt1, D217(OsHsp90) - K186(OsSgt1), D218(OsHsp90) - K237(OsSgt1), K161(OsHsp90) - E239 (OsSgt1). Our work revealed that salt bridges played vital roles in the complex stability,and the results would provide a crucial clue for a better understanding of the binding mechanisms between Hsp90 and Sgt1 in rice. More generally, the structural analysis might present opportunities in biologically engineering more adaptable rice grains.

Acknowledgments This work was supported by National Nature Science Foundation of China (30971740, 30821064). We acknowledge professor David Case for the kind gift of AMBER 11 software.

References

1. Emelyanov VV (2002) Phylogenetic relationships of organellar Hsp90 homologs reveal fundamental differences to organellar Hsp70 and Hsp60 evolution. Gene 299:125–133
2. Siligardi G, Hu B, Panaretou B, Piper PW, Pearl LH, Prodromou C (2004) Co-chaperone regulation of conformational switching in the Hsp90 ATPase cycle. J Biol Chem 279:51989–51998
3. Rutherford SL, Lindquist S (1998) Hsp90 as a capacitor for morphological evolution. Nature 396:336–342
4. Richter K, Buchner J (2001) Hsp90: chaperoning signal transduction. J Cell Physiol 188:281–290
5. Whitesell L, Lindquist SL (2005) HSP90 and the chaperoning of cancer. Nat Rev Cancer 5:761–772
6. Csermely P, Schnaider T, Soti C, Prohaszka Z, Nardai G (1998) The 90-kDa molecular chaperone family: structure, function, and clinical applications. A comprehensive review. Pharmacol Ther 79:129–168
7. Kabakov AE, Kudryavtsev VA, Gabai VL (2010) Hsp90 inhibitors as promising agents for radiotherapy. J Mol Med (Berl) 88:241–247
8. Janin YL (2010) ATPase inhibitors of heat-shock protein 90, second season. Drug Discov Today 15:342–353
9. Joab I et al (1984) Common non-hormone binding component in non-transformed chick oviduct receptors of four steroid hormones. Nature 308:850–853
10. Wilhelmsson A, Cuthill S, Denis M, Wikstrom AC, Gustafsson JA, Poellinger L (1990) The specific DNA binding activity of the dioxin receptor is modulated by the 90 kd heat shock protein. EMBO J 9:69–76
11. Wegele H, Muller L, Buchner J (2004) Hsp70 and Hsp90–a relay team for protein folding. Rev Physiol Biochem Pharmacol 151:1–44
12. Azevedo C, Sadanandom A, Kitagawa K, Freialdenhoven A, Shirasu K, Schulze-Lefert P (2002) The RAR1 interactor SGT1, an essential component of R gene-triggered disease resistance. Science 295:2073–2076
13. Steensgaard P et al (2004) Sgt1 is required for human kinetochore assembly. EMBO Rep 5:626–631
14. Mayor A, Martinon F, De Smedt T, Petrilli V, Tschopp J (2007) A crucial function of SGT1 and HSP90 in inflammasome activity links mammalian and plant innate immune responses. Nat Immunol 8:497–503
15. Azevedo C et al (2006) Role of SGT1 in resistance protein accumulation in plant immunity. EMBO J 25:2007–2016
16. Noel LD et al (2007) Interaction between SGT1 and cytosolic/nuclear HSC70 chaperones regulates Arabidopsis immune responses. Plant Cell 19:4061–4076
17. Kadota Y, Amigues B, Ducassou L, Madaoui H, Ochsenbein F, Guerois R, Shirasu K (2008) Structural and functional analysis of SGT1-HSP90 core complex required for innate immunity in plants. EMBO Rep 9:1209–1215
18. Lee YT, Jacob J, Michowski W, Nowotny M, Kuznicki J, Chazin WJ (2004) Human Sgt1 binds HSP90 through the CHORD-Sgt1 domain and not the tetratricopeptide repeat domain. J Biol Chem 279:16511–16517
19. Boter M et al (2007) Structural and functional analysis of SGT1 reveals that its interaction with HSP90 is required for the accumulation of Rx, an R protein involved in plant immunity. Plant Cell 19:3791–3804
20. Zhang M et al (2008) Structural and functional coupling of Hsp90- and Sgt1-centred multi-protein complexes. EMBO J 27:2789–2798
21. Zhang Y, Baaden M, Yan J, Shao J, Qiu S, Wu Y, Ding Y (2010) The molecular recognition mechanism for superoxide dismutase presequence binding to the mitochondrial protein import receptor Tom20 from Oryza sativa involves an LRTLA motif. J Phys Chem B 114:13839–13846
22. Gohlke H, Kiel C, Case DA (2003) Insights into protein-protein binding by binding free energy calculation and free energy decomposition for the Ras-Raf and Ras-RalGDS complexes. J Mol Biol 330:891–913
23. Gohlke H, Case DA (2004) Converging free energy estimates: MM-PB(GB)SA studies on the protein-protein complex Ras-Raf. J Comput Chem 25:238–250
24. Thompson JD, Gibson TJ, Higgins DG (2002) Multiple sequence alignment using ClustalW and ClustalX. Curr Protoc Bioinformatics Chapter 2:Unit 2 3
25. Kollman PA et al (2000) Calculating structures and free energies of complex molecules: combining molecular mechanics and continuum models. Acc Chem Res 33:889–897
26. Tsui V, Case DA (2000) Theory and applications of the generalized Born solvation model in macromolecular simulations. Biopolymers 56:275–291
27. Yi H, Qiu S, Cao Z, Wu Y, Li W (2008) Molecular basis of inhibitory peptide maurotoxin recognizing Kv1.2 channel explored by ZDOCK and molecular dynamic simulations. Proteins 70:844–854
28. Yi H, Cao Z, Yin S, Dai C, Wu Y, Li W (2007) Interaction simulation of hERG K + channel with its specific BeKm-1 peptide: insights into the selectivity of molecular recognition. J Proteome Res 6:611–620

29. Wu Y, Cao Z, Yi H, Jiang D, Mao X, Liu H, Li W (2004) Simulation of the interaction between ScyTx and small conductance calcium-activated potassium channel by docking and MM-PBSA. Biophys J 87:105–112
30. Qiu S, Yi H, Liu H, Cao Z, Wu Y, Li W (2009) Molecular Information of charybdotoxin blockade in the large conductance calcium-activated potassium channel. J Chem Inf Model 49:1831–1838
31. Case DA et al (2005) The Amber biomolecular simulation programs. J Comput Chem 26:1668–1688
32. Hornak V, Abel R, Okur A, Strockbine B, Roitberg A, Simmerling C (2006) Comparison of multiple Amber force fields and development of improved protein backbone parameters. Proteins 65:712–725
33. Larini L, Mannella R, Leporini D (2007) Langevin stabilization of molecular-dynamics simulations of polymers by means of quasi-symplectic algorithms. J Chem Phys 126:104101
34. Qiu D, Shenkin P, Hollinger F, Still C (1997) The GB/SA Continuum Model for Solvation. A fast analytical method for the calculation of approximate born radii. J Phys Chem A 101:3005–3014
35. Tsui V, Case DA (2000) Molecular dynamics simulations of nucleic acids with a generalized born solvation model. J Am Chem Soc 122:2489–2498
36. Van Der Spoel D, Lindahl E, Hess B, Groenhof G, Mark AE, Berendsen HJ (2005) GROMACS: fast, flexible, and free. J Comput Chem 26:1701–1718
37. Jorgensen WL, Maxwell DS, Tirado-Rives J (1996) Development and testing of the OPLS All-Atom force field on conformational energetics and properties of organic liquids. J Am Chem Soc 118:11225–11236
38. Berendsen HJCPJ, van Gunsteren WF, DiNola A, Haak JR (1984) Molecular dynamics with coupling to an external bath. J Chem Phys 81:3584–3590
39. Essmann U, Perera L, Berkowitz ML, Darden T, Lee H, Pedersen LG (1995) A smooth particle mesh Ewald method. J Chem Phys 103:8577–8593
40. Hess BBH, Berendsen HJC, Fraaije JGEM (1997) LINC: a linear constraint solver for molecular simulations. J Comput Chem 18:1463–1472
41. Humphrey W, Dalke A, Schulten K (1996) VMD: visual molecular dynamics. J Mol Graph 14(33–38):27–38